Journal of Sound and Vibration (2002) **253**(2), 421–445
doi:10.1006/jsvi.2001.4062, available online at http://www.idealibrary.com on IDEAL®

AN EXTENSION OF COMPLEX MODES FOR THE RESOLUTION OF FINITE-ELEMENT POROELASTIC PROBLEMS

O. Dazel and F. Sgard

Laboratoire des Sciences de l'Habitat, DGCB URA CNRS 1652, *Ecole Nationale des Travaux Publics de l'Etat, Rue Maurice Audin, F*-69518 *Vaulx-en-Velin Cedex, France*

C.-H. Lamarque

Laboratoire Géo-Matériaux, DGCB URA CNRS 1652, *Ecole Nationale des Travaux Publics de l'Etat, Rue Maurice Audin, F*-69518 *Vaulx-en-Velin Cedex, France. E-mail: claude.lamarque@entpe.fr*

and

N. Atalla

GAUS, Mech. Eng., Univ. de Sherbrooke, QC, Canada

(*Received* 8 *February* 2001, *and in final form* 27 *September* 2001)

A new modal synthesis technique inspired from complex modes is presented in this paper. The purpose of this method is to find an alternative to the weakness of usual modal techniques in order to improve resolution of finite-element poroelastic problems. Firstly, the construction of modes and the synthesis for a general forcing is explained. Secondly, the approach is applied to a one-dimensional poroelastic problem. Finally, the approach is numerically tested and its performance is investigated by comparison with solutions obtained with a direct resolution of the system.

1. INTRODUCTION

Finite multi-layer poroelastic structures are used to improve noise control in many engineering fields such as aeronautics, automobiles, etc. To predict the vibro-acoustic behavior of such systems, several finite-element models have been implemented [1–5] that use $\{\mathbf{u}, \mathbf{U}\}$ formulation of Biot's poroelasticity equations [6, 7]. However, it has been shown that $\{\mathbf{u}, \mathbf{U}\}$ formulation requires cumbersome calculations for large finite-element models. Mixed formulations (displacement of solid phase, pressure in the pores of fluid phase) have been introduced [8, 9]. Atalla *et al.* gave an exact $\{\mathbf{u}, \mathbf{P}\}$ formulation (with no new assumptions beyond those governing Biot's poroelastic equations) for a harmonic motion thereby reducing the number of variables from 6 to 4. This formulation exhibits some advantages compared to $\{\mathbf{u}, \mathbf{U}\}$: the stiffness matrix associated with the solid phase is frequency independent and it accounts naturally for poroelastic–poroelastic interfaces. Nevertheless, systems may be still large sized even for simple systems (if a large frequency band is considered) or for complicated systems (e.g., multilayered). Therefore, there is a need to find numerical techniques in order to improve the solving process. At low frequencies, modal synthesis [10] is commonly used to solve for the vibration of fluid structure interaction problems [11–18]. Modal analysis is based on two important properties of

0022-460X/02/$35.00

natural modes: the *orthogonality property* and the *reduction property*. The first one allows one to express an n-d.o.f. system in terms of n time-dependent uncoupled co-ordinates describing the motion of the system at any time. The *reduction property* is based on the physical property that a small number of modes are needed to represent the dynamic behavior of the system. Unfortunately, classical modal analysis cannot be applied to the poroelastic problem because of the frequency non-linearity of the associated eigenvalue problem [5]. Attempts have been made by authors to use modal techniques to solve poroelastic problems. Bouhioui and Hodgson [19] split the spectrum into frequency bands over which the eigenvalue problem was supposed to be frequency independent. This allowed them to construct a modal basis for each frequency band. Sgard and Atalla [20, 21] used an expansion of the $\{\mathbf{u}, \mathbf{P}\}$ variables in terms of the uncoupled undamped modes of each phase. However, this leads to convergence problem due to the fact that damping mechanisms associated with the porous material and coupling between both phases were not accounted for in the modal analysis.

The purpose of this paper is to propose a new modal analysis approach based on an extension of the complex modes technique to calculate the vibro-acoustic behavior of a porous material. The originality of this approach is to exhibit coupled modes which take into account thermal and viscous damping mechanisms present in the poroelastic material. It will be shown that this technique leads to a reduction of the size of the problem.

Section 2 presents finite-element equations related to poroelastic problems. Sections 3 and 4 are devoted to the description of the generalized complex modes synthesis. This technique is applied to the poroelastic problem in section 5. Finally, section 6 presents numerical results and section 7 gives the conclusion of this work.

2. THE POROELASTIC PROBLEM

The finite-element discretization of the Biot $\{\mathbf{u}, \mathbf{P}\}$ weak integral formulation at pulsation ω is given by Atalla *et al.* [8] as

$$\begin{bmatrix} [\tilde{\mathbf{K}}] + (\mathrm{j}\omega)^2[\tilde{\mathbf{M}}] & -[\tilde{\mathbf{C}}] \\ -\omega^2[\tilde{\mathbf{C}}]^{\mathrm{t}} & [\tilde{\mathrm{H}}] - \omega^2[\tilde{\mathrm{Q}}] \end{bmatrix} \begin{Bmatrix} \mathbf{u} \\ \mathbf{P} \end{Bmatrix} \mathrm{e}^{\mathrm{j}\omega t} = \begin{Bmatrix} \mathbf{F}^s \\ \mathbf{F}^f \end{Bmatrix} \mathrm{e}^{\mathrm{j}\omega t}, \tag{1}$$

where $\mathbf{u}$ is the displacement nodal vector of the solid phase, $\mathbf{P}$ is the interstitial pressure nodal vector of the fluid phase. $\mathbf{F}^s$ and $\mathbf{F}^f$ are, respectively, the forcing applied on the solid and the fluid phases. $[\tilde{\mathbf{K}}]$ and $[\tilde{\mathbf{M}}]$ represent the stiffness and mass matrices of the solid phase which are given by

$$[\tilde{\mathbf{K}}] = (1 + \mathrm{j}\eta_s)[\mathbf{K}_{int}] \text{ with } [\mathbf{K}_{int}] = \int_{\Omega_p} [[\mathscr{L}][\mathbf{N}^u]]^{\mathrm{t}}[\mathbf{H}][\mathscr{L}][\mathbf{N}^u]\,\mathrm{d}\Omega; \tag{2}$$

$$[\tilde{\mathbf{M}}] = \tilde{\rho}[\mathbf{M}_{int}] \text{ with } [\mathbf{M}_{int}] = \int_{\Omega_p} [\mathbf{N}^u]^{\mathrm{t}}[\mathbf{N}^u]\,\mathrm{d}\Omega, \tag{3}$$

where Ω_p is the porous volume, η_s is the structural damping coefficient and $\tilde{\rho}$ is the effective density of the solid phase. $[\mathbf{N}^u]$ and $[\mathbf{N}^p]$ are the elements' shape functions used to approximate the solid-phase displacement vector and the interstitial pressure respectively.

$[\mathbf{H}]$ is the Hooke's matrix of the solid phase and $[\mathscr{L}]$ is defined by

$$[\mathscr{L}] = \begin{bmatrix} \dfrac{\partial}{\partial x} & 0 & 0 & \dfrac{\partial}{\partial y} & 0 & \dfrac{\partial}{\partial z} \\ 0 & \dfrac{\partial}{\partial y} & 0 & \dfrac{\partial}{\partial x} & \dfrac{\partial}{\partial z} & 0 \\ 0 & 0 & \dfrac{\partial}{\partial z} & 0 & \dfrac{\partial}{\partial y} & \dfrac{\partial}{\partial x} \end{bmatrix}. \tag{4}$$

$[\tilde{\mathbf{H}}]$ and $[\tilde{\mathbf{Q}}]$ represent the kinetic and compression energy matrices of the fluid phase:

$$[\tilde{\mathbf{H}}] = \frac{h^2}{\tilde{\rho}_{22}}[\mathbf{H}_{int}] \text{ with } [\mathbf{H}_{int}] = \int_{\Omega_p} \nabla[\mathbf{N}^p]^{\mathrm{t}} \nabla[\mathbf{N}^p] \, \mathrm{d}\Omega, \tag{5}$$

$$[\tilde{\mathbf{Q}}] = \frac{h^2}{\tilde{R}}[\mathbf{Q}_{int}] \text{ with } [\mathbf{Q}_{int}] = \int_{\Omega_p} [\mathbf{N}^p]^{\mathrm{t}}[\mathbf{N}^p] \, \mathrm{d}\Omega. \tag{6}$$

Here h denotes the porosity. $\tilde{R}$ may be interpreted as the bulk modulus of the air occupying a fraction h of a unit volume of aggregate and $\tilde{\rho}_{22}$ is the modified Biot's density of the fluid phase. The expressions of $\tilde{\rho}$ and $\tilde{\rho}_{22}$ are given by

$$\tilde{\rho} = \tilde{\rho}_{11} - \frac{\tilde{\rho}_{12}^2}{\tilde{\rho}_{22}}, \qquad \tilde{\rho}_{22} = \rho_{22} + \frac{\tilde{b}}{\mathrm{j}\omega}, \tag{7}$$

with

$$\tilde{\rho}_{11} = \rho_{11} + \frac{\tilde{b}}{\mathrm{j}\omega}, \qquad \tilde{\rho}_{12} = \rho_{12} - \frac{\tilde{b}}{\mathrm{j}\omega} \tag{8}$$

and

$$\rho_{11} = (1-h)\rho_s - \rho_{12}, \quad \rho_{22} = h\rho_f - \rho_{12}, \quad \rho_{12} = -h\rho_f(\alpha_\infty - 1). \tag{9}$$

ρ_s and ρ_f are, respectively, the mass density of the solid phase and of the fluid in the pores and α_∞ is the tortuosity [22]. $\tilde{\rho}_{11}$ is the modified Biot's density of the solid phase accounting for viscous dissipation and $\tilde{\rho}_{12}$ accounts for the interaction between the inertia forces of the solid and fluid phases together with viscous dissipation. $\tilde{b}$ is a frequency-dependent viscous coefficient defined by

$$\tilde{b} = h^2\sigma\tilde{G}, \qquad \tilde{G} = \sqrt{1 + \mathrm{j}\omega/H}, \qquad H = \sigma^2\Lambda^2h^2/4\alpha_\infty^2\eta\rho_f,$$

where σ is the flow resistivity, H is the viscous characteristic frequency [5], Λ is the viscous characteristic length introduced by Johnson [23] and η is the kinematic fluid viscosity. Note that $\tilde{G}$ accounts for viscous effects.

Finally, $[\tilde{\mathbf{C}}]$ is a volume coupling matrix between the solid-phase displacement and the fluid-phase pressure:

$$[\tilde{\mathbf{C}}] = \tilde{\gamma}[\mathbf{C}_{int}] \text{ with } [\mathbf{C}_{int}] = \int_{\Omega_p} [\mathbf{N}^u]^{\mathrm{t}} \nabla[\mathbf{N}^p] \, \mathrm{d}\Omega. \tag{10}$$

$\tilde{\gamma}$ is a coupling parameter:

$$\tilde{\gamma} = h\left(\frac{\tilde{\rho}_{12}}{\tilde{\rho}_{22}} - \frac{\tilde{Q}}{\tilde{R}}\right). \tag{11}$$

Note that for most of the porous materials, one has [8]

$$\tilde{Q} = (1-h)\tilde{K}_e, \qquad \tilde{R} = h\tilde{K}_e. \tag{12}$$

$\tilde{K}_e$ is the effective bulk modulus of the air in the pores [7] which accounts for thermal effects:

$$\tilde{K}_e = \frac{\gamma P_0}{\gamma - ((\gamma-1)/[1 + (H'/2\mathrm{j}\omega)\tilde{G}'])}, \qquad \tilde{G}' = \sqrt{1 + \frac{\mathrm{j}\omega}{H'}}, \qquad H' = \frac{16\eta}{\mathrm{Pr}\,\Lambda'^2\rho_f}. \tag{13}$$

H' is the thermal characteristic frequency given by Panneton [5], Λ' is the thermal characteristic length [24] and Pr is the Prandtl number. (A list of notations is given in Appendix A).

The matrix in the left-hand side of equation (1) is not symmetric. Nevertheless, one can give it a symmetric form by multiplying the set of equations related to the skeleton by $(\mathrm{j}\omega)^2$ and the set of equation related to the fluid phase by -1. Hence,

$$\begin{bmatrix} (\mathrm{j}\omega)^2[\tilde{\mathbf{K}}] + (\mathrm{j}\omega)^4[\tilde{\mathbf{M}}] & -(\mathrm{j}\omega)^2[\tilde{\mathbf{C}}] \\ -(\mathrm{j}\omega)^2[\tilde{\mathbf{C}}]^{\mathrm{t}} & -[\tilde{\mathbf{H}}] - (\mathrm{j}\omega)^2[\tilde{\mathbf{Q}}] \end{bmatrix} \begin{Bmatrix} \mathbf{u} \\ \mathbf{P} \end{Bmatrix} \mathrm{e}^{\mathrm{j}\omega t} = \begin{Bmatrix} (\mathrm{j}\omega)^2\mathbf{F}^s \\ -\mathbf{F}^f \end{Bmatrix} \mathrm{e}^{\mathrm{j}\omega t}. \tag{14}$$

Each matrix (except $[\tilde{\mathbf{K}}]$) represented with the symbol $\tilde{}$ is equal to the product of a complex function of the real parameter ω by a real symmetric matrix. The frequency non-linearity of the associated eigenvalue problem is induced by two effects. The first one is due to the frequency dependence of the coefficients $\tilde{\rho}$, $1/\tilde{\rho}_{22}$, $1/\tilde{R}$ and $\tilde{\gamma}$. The second one is induced by the selected $\{\mathbf{u}, \mathbf{P}\}$ formulation and the multiplication by powers of $(\mathrm{j}\omega)$ of these different coefficients. Figure 1 presents the variation of $|(\mathrm{j}\omega)^4\tilde{\rho}|$, $|h^2/\tilde{\rho}_{22}|$, $|(\mathrm{j}\omega)^2 h^2/\tilde{R}|$ and $|(\mathrm{j}\omega)^2\tilde{\gamma}|$ for the three materials presented in section 5 in the frequency range [1; 1500 Hz]. Furthermore, all these functions have the highlighting property of being regular enough to be expressed at low frequencies by a Taylor expansion with real coefficients. Note that matrix $[\tilde{\mathbf{K}}]$ contains the hysteretic damping of the solid phase which will be neglected for the modes calculation. All these considerations will be detailed in section 5.

All the variables $\tilde{\rho}$, $h^2/\tilde{\rho}_{22}$, $h^2/\tilde{R}$ and $\tilde{\gamma}$ can be expanded in the following form:

$$\tilde{V} = \sum_{i=0}^{d} v_i(\mathrm{j}\omega)^i + O(\omega^{d+1}). \tag{15}$$

This induces that each one of the matrices appearing in equations (2), (3), (5), (6), (10) can be written as

$$[\tilde{\mathbf{M}}] = \sum_{i=0}^{d} m_i(\mathrm{j}\omega)^i[\mathbf{M}_{int}] + O(\omega^{d+1}), \quad [\tilde{\mathbf{K}}] = \sum_{i=0}^{d} k_i(\mathrm{j}\omega)^i[\mathbf{K}_{int}] + O(\omega^{d+1}), \tag{16a}$$

$$[\tilde{\mathbf{H}}] = \sum_{i=0}^{d} h_i(\mathrm{j}\omega)^i[\mathbf{H}_{int}] + O(\omega^{d+1}), \quad [\tilde{\mathbf{Q}}] = \sum_{i=0}^{d} q_i(\mathrm{j}\omega)^i[\mathbf{Q}_{int}] + O(\omega^{d+1}), \tag{16b}$$

$$[\tilde{\mathbf{C}}] = \sum_{i=0}^{d} c_i(\mathrm{j}\omega)^i[\mathbf{C}_{int}] + O(\omega^{d+1}), \tag{16c}$$

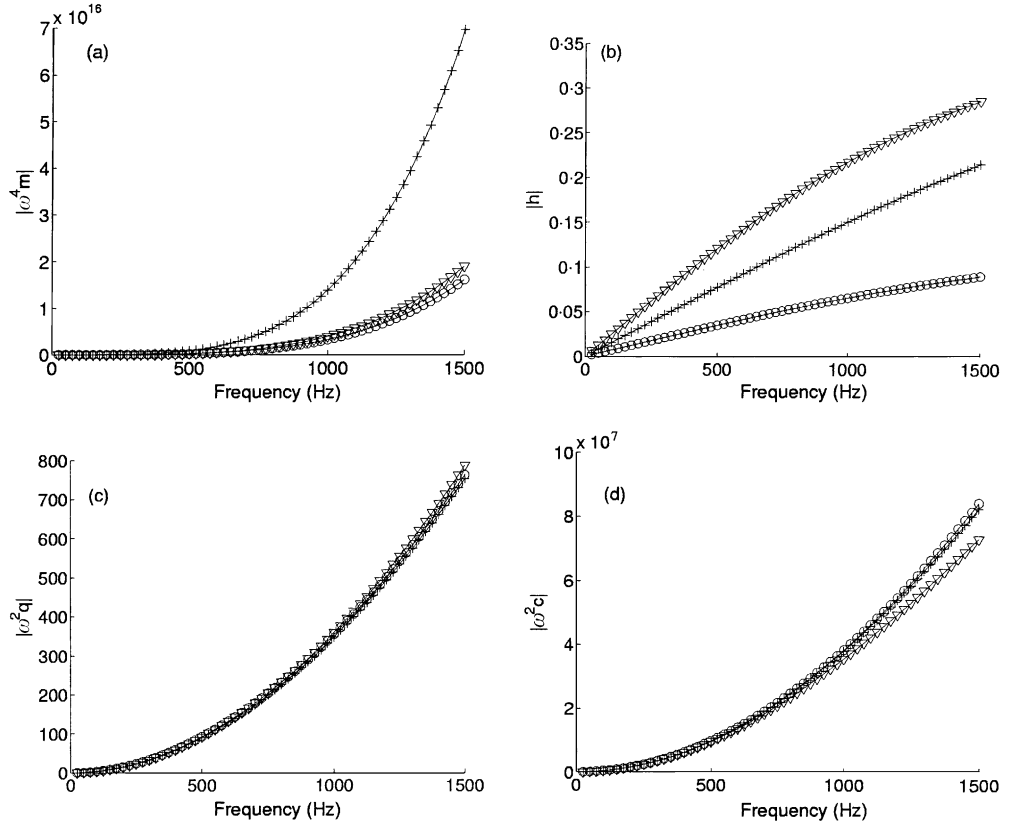

Figure 1. Coefficients versus frequency: (a) $\omega^4\tilde{\rho}$; (b) $h^2/\tilde{\rho}_{22}$; (c) $\omega^2(h^2/\tilde{R})$; (d) $\omega^2\tilde{\gamma}$; —○—, material A; —+—, material B; —▽—, material C.

where m_i, k_i, h_i, q_i and c_i are the coefficients of the Taylor expansions of $\tilde{\rho}$, 1, $h^2/\tilde{\rho}_{22}$, $h^2/\tilde{R}$ and $\tilde{\gamma}$ respectively.

Equation (14) can then be transformed as

$$\sum_{i=0}^{d} [\mathbf{M}_i](\mathrm{j}\omega)^i \begin{Bmatrix} \mathbf{u} \\ \mathbf{P} \end{Bmatrix} + [\mathscr{R}_d](\omega) \begin{Bmatrix} \mathbf{u} \\ \mathbf{P} \end{Bmatrix} = \begin{Bmatrix} \mathbf{F}'_s \\ \mathbf{F}'_p \end{Bmatrix}, \tag{17}$$

with the following matrices:

$$[\mathbf{M}_0] = \begin{bmatrix} [\mathbf{0}] & [\mathbf{0}] \\ [\mathbf{0}] & -h_0[\mathbf{H}_{int}] \end{bmatrix}, \qquad [\mathbf{M}_1] = \begin{bmatrix} [\mathbf{0}] & [\mathbf{0}] \\ [\mathbf{0}] & -h_1[\mathbf{H}_{int}] \end{bmatrix}, \tag{18, 19}$$

$$[\mathbf{M}_2] = \begin{bmatrix} k_0[\mathbf{K}_{int}] & -c_0[\mathbf{C}_{int}] \\ -c_0[\mathbf{C}_{int}]^{\mathrm{t}} & -h_2[\mathbf{H}_{int}] - q_0[\mathbf{Q}_{int}] \end{bmatrix}, \tag{20}$$

$$[\mathbf{M}_3] = \begin{bmatrix} [\mathbf{0}] & -c_1[\mathbf{C}_{int}] \\ -c_1[\mathbf{C}_{int}]^{\mathrm{t}} & -h_3[\mathbf{H}_{int}] - q_1[\mathbf{Q}_{int}] \end{bmatrix}, \tag{21}$$

$$[\mathbf{M}_i] = \begin{bmatrix} m_{i-4}[\mathbf{M}_{int}] & -c_{i-2}[\mathbf{C}_{int}] \\ -c_{i-2}[\mathbf{C}_{int}]^{\mathrm{t}} & -h_i[\mathbf{H}_{int}] - q_{i-2}[\mathbf{Q}_{int}] \end{bmatrix} \quad (i \geqslant 4), \tag{22}$$

where d corresponds to the order of Taylor expansion in terms of ω. Each $[\mathbf{M}_i]$ is a real symmetric matrix and $[\mathscr{R}_d](\omega)$ is a matrix depending on ω corresponding to the remainder. Under this form, equation (17) can be seen as an extension of the complex modes and the presentation of a new modal technique is the purpose of next section.

3. GENERALIZED COMPLEX MODES

In this section, an extension of the complex modes method [10] is presented. To the author's knowledge, this technique has never been expounded before. This presentation is made in a general case and its application to the poroelastic problem is the subject of section 5.

3.1. DEFINITIONS

Consider the equation

$$\mathscr{D}\mathbf{u} = \mathbf{0}, \tag{23}$$

where $\mathbf{u} \in \mathscr{C}^d(\mathbb{R}, \mathbb{C}^n)$, $d \in \mathbb{N}$ and $\mathscr{D}$ is a differential operator generally non-linear from $\mathscr{F}(\mathbb{R}, \mathbb{C}^n)$ into itself. It is assumed that $\mathscr{D}$ can be written in the form

$$\mathscr{D}\mathbf{u} = \sum_{i=0}^{d} [\mathbf{M}_i]\mathbf{u}^{(i)} + \mathscr{R}_d\mathbf{u}, \tag{24}$$

where $[\mathbf{M}_i]$ is a real symmetric (n, n) matrix, $\mathbf{u}^{(i)}$ is the ith derivative of $\mathbf{u}$ and $\mathscr{R}_d$ is an operator, called *remainder at order d*, from $\mathscr{C}^d(\mathbb{R}, \mathbb{C}^n)$ into $\mathscr{F}(\mathbb{R}, \mathbb{C}^n)$. The first part of the right-hand side is said to be the *expansion at order d*. It is further assumed that $det\,[\mathbf{M}_d] \neq 0$.

The idea of the approach is to find the modes of the *expansion at order d*.

3.2. PROBLEM TRANSFORMATION

The following equation is considered:

$$\sum_{i=0}^{d} [\mathbf{M}_i]\mathbf{u}^{(i)} = 0. \tag{25}$$

This problem of degree d and dimension n is transformed into a linear problem of dimension nd. We introduce $\mathbf{U} \in \mathscr{F}(\mathbb{R}, \mathbb{N}^{nd})$ assembled according to the model of Duncan's transformation [25]:

$$\mathbf{U} = \begin{Bmatrix} \mathbf{u}^{(d-1)} \\ \vdots \\ \mathbf{u}^{(1)} \\ \mathbf{u} \end{Bmatrix}. \tag{26}$$

$\mathbf{U}$ is called the associated generalized state vector of order $(d-1)$. $[\mathbf{A}]$ and $[\mathbf{B}]$ are constructed by block choosing equation (25) for the first relation. The choice of the $n(d-1)$

other relations is arbitrary. It is straightforward to show that solutions of equation (30) do not depend on this choice. The general form of the problem is then

$$\begin{bmatrix} [\mathbf{L}] & [\mathbf{M}_0] \\ [\mathbf{\Gamma}] & [\mathbf{0}] \end{bmatrix} \mathbf{U} = \begin{bmatrix} -[\mathbf{M}_d] & [\mathbf{0}] \\ [\mathbf{0}] & [\mathbf{\Gamma}] \end{bmatrix} \dot{\mathbf{U}}, \tag{27}$$

where $\dot{\mathbf{U}}$ denotes the first derivative of $\mathbf{U}$,

$$[\mathbf{L}] = [[\mathbf{M}_{d-1}] \quad \cdots \quad [\mathbf{M}_1]] \tag{28}$$

and $[\mathbf{\Gamma}]$ is an $(n(d-1), n(d-1))$ matrix to be chosen. With

$$[\mathbf{A}] = \begin{bmatrix} [\mathbf{L}] & [\mathbf{M}_0] \\ [\mathbf{\Gamma}] & [\mathbf{0}] \end{bmatrix} \quad \text{and} \quad [\mathbf{B}] = \begin{bmatrix} -[\mathbf{M}_d] & [\mathbf{0}] \\ [\mathbf{0}] & [\mathbf{\Gamma}] \end{bmatrix}, \tag{29}$$

equation (27) reads

$$[\mathbf{B}]\dot{\mathbf{U}} = [\mathbf{A}]\mathbf{U}. \tag{30}$$

Note that the solution of equations (27) is equivalent to solving

$$\begin{bmatrix} -[\mathbf{M}_d]^{-1}[\mathbf{L}] & -[\mathbf{M}_d]^{-1}[\mathbf{M}_0] \\ [\mathbf{I}_{n(d-1)}] & [\mathbf{0}] \end{bmatrix} \mathbf{U} = \dot{\mathbf{U}}, \tag{31}$$

where $[\mathbf{I}_{n(d-1)}]$ denotes the identity matrix of order $n(d-1)$.

In order to prove the orthogonality properties of modes, it is advantageous to choose $[\mathbf{\Gamma}]$ to make $[\mathbf{A}]$ and $[\mathbf{B}]$ symmetric as

$$\begin{bmatrix} [\mathbf{M}_{d-1}] & [\mathbf{M}_{d-2}] & \cdots & [\mathbf{M}_0] \\ [\mathbf{M}_{d-2}] & \cdots & [\mathbf{M}_0] & [\mathbf{0}] \\ \vdots & \vdots & \ddots & \vdots \\ [\mathbf{M}_0] & [\mathbf{0}] & \cdots & [\mathbf{0}] \end{bmatrix} \mathbf{U} = \begin{bmatrix} -[\mathbf{M}_d] & [\mathbf{0}] & \cdots & [\mathbf{0}] \\ [\mathbf{0}] & [\mathbf{M}_{d-2}] & \cdots & [\mathbf{M}_0] \\ \vdots & \vdots & \ddots & \vdots \\ [\mathbf{0}] & [\mathbf{M}_0] & \cdots & [\mathbf{0}] \end{bmatrix} \dot{\mathbf{U}}. \tag{32}$$

Equation (32) is solved by looking for solutions of the form $\mathbf{u}(t) = \mathbf{u}_0 e^{st}$ where $\mathbf{u}_0 \in \mathbb{C}^n$ and $s \in \mathbb{C}$. A classical eigenvalue problem is then obtained:

$$s[\mathbf{B}]\mathbf{U}_0 = [\mathbf{A}]\mathbf{U}_0. \tag{33}$$

Since $[\mathbf{A}]$ and $[\mathbf{B}]$ are real

$$([\mathbf{A}] - s[\mathbf{B}])\mathbf{U}_0 = \mathbf{0} \Leftrightarrow ([\mathbf{A}] - \bar{s}[\mathbf{B}])\bar{\mathbf{U}}_0 = \mathbf{0}. \tag{34}$$

Therefore, if $(s, \mathbf{U}_0)$ is solution of equation (33), the conjugate, $(\bar{s}, \bar{\mathbf{U}}_0)$ is also a solution of equation (33).

3.3. EIGENVECTORS' ORTHOGONALITY

Let $(s_i, \mathbf{U}_i)$ and $(s_j, \mathbf{U}_j)$ be two solutions of equation (33) so that $s_i \neq s_j$; then one can write

$$([\mathbf{A}] - s_i[\mathbf{B}])\mathbf{U}_i = \mathbf{0}, \qquad ([\mathbf{A}] - s_j[\mathbf{B}])\mathbf{U}_j = \mathbf{0}. \tag{35, 36}$$

By projection, one has

$$\mathbf{U}_j^t[\mathbf{A}]\mathbf{U}_i - s_i\mathbf{U}_j^t[\mathbf{B}]\mathbf{U}_i = 0 \tag{37}$$

and

$$\mathbf{U}_i^t[\mathbf{A}]\mathbf{U}_j - s_j\mathbf{U}_i^t[\mathbf{B}]\mathbf{U}_j = 0. \tag{38}$$

Due to the symmetry of $[\mathbf{A}]$ and $[\mathbf{B}]$ subtracting equation (37) from equation (38) yields

$$(s_j - s_i)\mathbf{U}_j^t[\mathbf{B}]\mathbf{U}_i = 0 \tag{39}$$

and hence,

$$\forall(i, j), \quad s_i \neq s_j \Rightarrow \mathbf{U}_j^t[\mathbf{B}]\mathbf{U}_i = 0 \tag{40}$$

and

$$\forall(i, j), \quad s_i \neq s_j \Rightarrow \mathbf{U}_j^t[\mathbf{A}]\mathbf{U}_i = 0. \tag{41}$$

In the case where $(s, \mathbf{U})$ and $(s, \mathbf{U}')$ are two different solutions of equation (32) the *degenerescence theorem* [26] cannot be applied because $[\mathbf{B}]$ is not a definite-positive matrix so that no scalar product can be defined with respect to $[\mathbf{B}]$. Nevertheless, theoretical properties of bi-orthogonality between the eigenmodes and its adjoint could be envisaged to generalize the orthogonality properties [27]. This will not be detailed in this part because in all the numerical cases multiple eigenvalues will correspond to modes that will be discarded.

4. MODAL SUPERPOSITION

4.1. NOTATIONS

First of all, to improve the readability of the text, all notations and conventions used in this part are presented. $[\mathbf{\Lambda}]$ is the diagonal matrix where the ith value corresponds to the ith eigenvalue of equation (33) and $[\mathbf{\Phi}]$ is a matrix where the ith column is the corresponding eigenvector of equation (33). The following decompositions of $[\mathbf{\Phi}]$ are considered:

$$[\mathbf{\Phi}] = \begin{bmatrix} [\mathbf{\Upsilon}] \\ [\boldsymbol{\psi}_0] \end{bmatrix} = \begin{bmatrix} [\boldsymbol{\psi}_{d-1}] \\ [\mathbf{\Xi}] \end{bmatrix}. \tag{42}$$

Here $[\boldsymbol{\psi}_i]$ is the (n, nd) matrix of the ith derivatives of the nd solutions of equation (25). $[\mathbf{\Upsilon}]$ and $[\mathbf{\Xi}]$ and $((d-1)n, nd)$ matrices. The following relations hold:

$$\forall_i \in [0, d-1], \qquad [\boldsymbol{\psi}_{i+1}] = [\boldsymbol{\psi}_i][\mathbf{\Lambda}], \tag{43}$$

$$[\mathbf{\Upsilon}] = [\mathbf{\Xi}][\mathbf{\Lambda}]. \tag{44}$$

The modal decomposition of vector $\mathbf{U}$ using the modal basis $[\mathbf{\Phi}] = [\phi_i]$ reads

$$\mathbf{U} = \sum_{i=0}^{nd} z_i\boldsymbol{\phi}_i = [\mathbf{\Phi}]\mathbf{z}, \tag{45}$$

where vector $\mathbf{z}$ corresponds to the modal coefficients. Hence,

$$\mathbf{U} = \begin{bmatrix} [\Upsilon] \\ [\psi_0] \end{bmatrix} \mathbf{z}, \qquad \dot{\mathbf{U}} = \begin{bmatrix} [\psi_{d-1}] \\ [\Xi] \end{bmatrix} \dot{\mathbf{z}} \tag{46, 47}$$

and by identification

$$[\Upsilon]\mathbf{z} = [\Xi]\dot{\mathbf{z}}, \tag{48}$$

which follows from the redundancy of the Generalized State Vector.

4.2. FORCED DIFFERENTIAL PROBLEM

To present the forced differential problem, consider the equation

$$\mathscr{D}\mathbf{u} = \mathbf{f}, \tag{49}$$

where $\mathscr{D}$ is defined by equation (24); $\mathbf{f}$ is the forcing and pertains to $\mathscr{F}(\mathbb{R}, \mathbb{C}^n)$. This equation is rewritten in the Generalized State Space, with the notations of the former section, as

$$-[\mathbf{B}]\dot{\mathbf{U}} + [\mathbf{A}]\mathbf{U} + \mathscr{R}_1\mathbf{U} = \boldsymbol{\mu}, \tag{50}$$

with

$$\boldsymbol{\mu} = (\mathbf{f}^{\mathrm{t}}\mathbf{0}\cdots\mathbf{0})^{\mathrm{t}} \quad \text{and} \quad \mathscr{R}_1\mathbf{U} = (\mathscr{R}_d^{\mathrm{t}}\mathbf{u}\mathbf{0}\cdots\mathbf{0})^{\mathrm{t}}. \tag{51}$$

Hence by pre-multiplying equation (50) by $[\boldsymbol{\Phi}]^{\mathrm{t}}$ one gets

$$-[\boldsymbol{\Phi}]^{\mathrm{t}}[\mathbf{B}][\boldsymbol{\Phi}]\dot{\mathbf{z}} + [\boldsymbol{\Phi}]^{\mathrm{t}}[\mathbf{A}][\boldsymbol{\Phi}]\mathbf{z} + [\boldsymbol{\Phi}]^{\mathrm{t}}\mathscr{R}_1[\boldsymbol{\Phi}]\mathbf{z} = \mathbf{v}, \tag{52}$$

with

$$\mathbf{v} = [\boldsymbol{\Phi}]^{\mathrm{t}}\boldsymbol{\mu}. \tag{53}$$

4.2.1. *Case* 1: R_1 *is negligible*

The ith row of equation (52) reads

$$-\dot{z}_i + s_i z_i = v_i / \boldsymbol{\phi}^{i^{\mathrm{t}}}[\mathbf{B}]\boldsymbol{\phi}^i, \tag{54}$$

with

$$b_i = \boldsymbol{\phi}^{i^{\mathrm{t}}}[\mathbf{B}]\boldsymbol{\phi}^i. \tag{55}$$

One then obtains

$$z_i(t) = \frac{1}{b_i}\int_0^t v_i(\tau)\mathrm{e}^{s_i(t-\tau)}\,\mathrm{d}\tau. \tag{56}$$

Recalling equation (45), one has

$$\mathbf{u}(t) = \sum_{r=1}^{nd} \frac{1}{b_r}\boldsymbol{\psi}_0^r \int_0^t v_r(\tau)\mathrm{e}^{s_r(t-\tau)}\,\mathrm{d}\tau. \tag{57}$$

In order to use the *reduction property*, a sub-family $[\underline{\boldsymbol{\Phi}}]$ of $[\boldsymbol{\Phi}]$ has to be selected by keeping m modes in the nd of the modal basis. The selection process will be explained in section 5.3. Thus

$$[\underline{\boldsymbol{\Phi}}] = [\boldsymbol{\Phi}][\boldsymbol{\Theta}], \tag{58}$$

where $[\boldsymbol{\Theta}]$ is an (nd, m) matrix where the coefficient of index (i, j) is equal to 1 if the jth mode of $[\boldsymbol{\Phi}]$ is selected at the ith place. Let $[\underline{\psi_0}]$ be the selection of m modes among the nd of the modal basis:

$$[\underline{\psi_0}] = [\psi_0][\boldsymbol{\Theta}]. \tag{59}$$

Finally, one obtains

$$\{\underline{\mathbf{u}}\}(t) = \sum_{\underline{r}=1}^{m} \frac{1}{b_{\underline{r}}} \underline{\boldsymbol{\psi}_0^r} \int_0^t v_{\underline{r}}(\tau) \mathrm{e}^{s_{\underline{r}}(t-\tau)} \, \mathrm{d}\tau. \tag{60}$$

4.2.2. *Case 2: $\mathscr{R}_1$ is not negligible*

In some cases, particularly for porous materials, the contribution of $\mathscr{R}_1$ may be sufficiently important and the approximation of the former section cannot be applied. In the present case, the *orthogonality property* cannot be used and it is only possible to apply the *reduction property*. According to equation (52), a projection with respect to matrix $[\boldsymbol{\Phi}]$ has to be done. It is shown here that a projection with respect to matrix $[\psi_0]$ can be done, which is better in terms of number of operations. In particular, the projection does not depend on the order of the expansions.

From equations (27) and (42) one can write

$$[\boldsymbol{\Phi}]^{\mathrm{t}}[\mathbf{A}][\boldsymbol{\Phi}] = [[\boldsymbol{\psi}_{d-1}]^{\mathrm{t}}[\boldsymbol{\Xi}]^{\mathrm{t}}] \begin{bmatrix} [\mathbf{L}] & [\mathbf{M}_0] \\ [\boldsymbol{\Gamma}] & [\mathbf{0}] \end{bmatrix} \begin{bmatrix} [\boldsymbol{\Upsilon}] \\ [\psi_0] \end{bmatrix}$$

$$= [\boldsymbol{\psi}_{d-1}]^{\mathrm{t}}[[\mathbf{L}][\boldsymbol{\Upsilon}] + [\mathbf{M}_0][\psi_0]] + [\boldsymbol{\Xi}]^{\mathrm{t}}[\boldsymbol{\Gamma}][\boldsymbol{\Upsilon}] \tag{61}$$

and

$$[\boldsymbol{\Phi}]^{\mathrm{t}}[\mathbf{B}][\boldsymbol{\Phi}] = [[\boldsymbol{\psi}_{d-1}]^{\mathrm{t}}[\boldsymbol{\Xi}]^{\mathrm{t}}] \begin{bmatrix} -[\mathbf{M}_d] & [\mathbf{0}] \\ [\mathbf{0}] & [\boldsymbol{\Gamma}] \end{bmatrix} \begin{bmatrix} [\boldsymbol{\psi}_{d-1}] \\ [\boldsymbol{\Xi}] \end{bmatrix}$$

$$= -[\boldsymbol{\psi}_{d-1}]^{\mathrm{t}}[\mathbf{M}_d][\boldsymbol{\psi}_{d-1}] + [\boldsymbol{\Xi}]^{\mathrm{t}}[\boldsymbol{\Gamma}][\boldsymbol{\Xi}]. \tag{62}$$

Upon considering

$$\mathscr{R}_1 \mathbf{U}(t) = \mathscr{R}_1[\boldsymbol{\Phi}]\mathbf{z}(t) = \mathscr{R}_d\{[\psi_0]\mathbf{z}^{(i)}(t)\}, \tag{63}$$

equation (52) becomes

$$[\boldsymbol{\psi}_{d-1}]^{\mathrm{t}}[[\mathbf{M}_d][\boldsymbol{\psi}_{d-1}]\dot{\mathbf{z}}(t) + [\boldsymbol{\psi}_{d-1}]^{\mathrm{t}}[[\mathbf{L}][\boldsymbol{\Upsilon}] + [\mathbf{M}_0][\psi_0]]\mathbf{z}(t)$$

$$+ [\boldsymbol{\psi}_{d-1}]^{\mathrm{t}}\mathscr{R}_d\{[\psi_0]\mathbf{z}^{(i)}\}(t) = \mathbf{v}(t). \tag{64}$$

With

$$[\boldsymbol{\psi}_d]\mathbf{z} = [\boldsymbol{\psi}_{d-1}]\dot{\mathbf{z}}, \tag{65}$$

one gets

$$[\boldsymbol{\psi}_{d-1}]^{\mathrm{t}}[[\mathbf{M}_d][\boldsymbol{\psi}_d] + [\mathbf{L}][\boldsymbol{\Upsilon}] + [\mathbf{M}_0][\boldsymbol{\psi}_0]]\mathbf{z}(t)$$

$$+ [\boldsymbol{\psi}_{d-1}]^{\mathrm{t}}\mathscr{R}_d\{[\boldsymbol{\psi}_0]\mathbf{z}^{(i)}\}(t) = \mathbf{v}(t), \tag{66}$$

which is the projection of the initial problem on the $[\boldsymbol{\psi}_0]$ family:

$$[\boldsymbol{\Lambda}]^{d-1}[\boldsymbol{\psi}_0]^{\mathrm{t}}\mathscr{D}[\boldsymbol{\psi}_0]\mathbf{z}(t) = [\boldsymbol{\Lambda}]^{d-1}[\boldsymbol{\psi}_0]^{\mathrm{t}}\mathbf{f}(t). \tag{67}$$

An (nd, nd) linear system has to be solved for each t. Let $\boldsymbol{\zeta}(t)$ be the solution. The modal superposition then gives

$$\mathbf{u}(t) = [\boldsymbol{\psi}_0]\boldsymbol{\zeta}(t). \tag{68}$$

The solution of equation (67) involves solving an order m problem for each t:

$$[\underline{\boldsymbol{\Lambda}}]^{d-1}[\underline{\boldsymbol{\psi}_0}]^{\mathrm{t}}\mathscr{D}[\underline{\boldsymbol{\psi}_0}]\underline{\mathbf{z}}(t) = [\boldsymbol{\Lambda}]^{d-1}[\underline{\boldsymbol{\psi}_0}]^{\mathrm{t}}\mathbf{f}(t). \tag{69}$$

Let $\underline{\boldsymbol{\zeta}}(t)$ be the solution. An approximation $\underline{\mathbf{u}}$ of vector $\mathbf{u}$ is then given by

$$\underline{\mathbf{u}}(t) = [\underline{\boldsymbol{\psi}_0}]\underline{\boldsymbol{\zeta}}(t). \tag{70}$$

4.3. STABILITY OF THE SOLUTION

The stability of the approximate model (32) is not ensured in a general case and physical conditions need now to be considered. Unstable modes can appear and a procedure to filter them has to be elaborated. Fung *et al.* [28] inspired by Tam and Auriault [29] proposed, in the context of a time-domain impedance problem, a method which consists in replacing the initial unstable problem by an equivalent stable one determined either experimentally or analytically.

In our case, the stability of the modal solution (57) requires the real part of all the eigenvalues s_r to be negative. In the case of natural undamped modes, the nullity of the real part is proved by the positivity of the mass and stiffness matrices. Classical complex modes have been introduced in the scope of structural dynamics of viscously damped discrete system [30]. The related stability has been studied analytically [31] and is satisfied due to physical conditions.

In the case of generalized complex modes (24), results for the sign of the real part of the eigenvalues cannot be obtained without physical conditions. The authors are not aware of stability results regarding equation (32). Some indications on the stability of the model can, however, be given for the problem of interest. Indeed, the application of this technique to porous materials should not lead to modes with a positive real part by reason of the dissipative nature of poroelastic media. From a numerical point of view, the numerous simulations have shown that modes with a positive real part can be found though. The existence of these modes may be due to numerical errors in the modes' determination. Nevertheless, they all had a high eigenfrequency so that they were very far from the set of selected modes for the modal synthesis and then were not selected. The stability of the model is then ensured.

4.4. HARMONIC PROBLEMS

The temporal dependency $e^{j\omega t}$ is now assumed for all fields. This case corresponds to the poroelastic materials considered in sections 2 and 5.

Equation (49) becomes

$$\hat{\mathscr{D}}(\omega)\hat{\mathbf{u}}e^{j\omega t} = \hat{\mathbf{f}}e^{j\omega t}, \tag{71}$$

where $\hat{\mathscr{D}}$ is such that

$$\hat{\mathscr{D}}(\omega)\hat{\mathbf{u}} = \sum_{i=0}^{d} [\mathbf{M}_i](j\omega)^i\hat{\mathbf{u}} + \hat{\mathscr{R}}_d(\omega)\hat{\mathbf{u}}, \tag{72}$$

where each $[\mathbf{M}_i]$ is a real symmetric (n, n) matrix. $det[\mathbf{M}_d] \neq 0$ is assumed.

4.4.1. *Case* 1: $\hat{\mathscr{R}}_1$ *is negligible*

Equation (57) gives

$$\hat{\mathbf{u}} = \sum_{r=1}^{nd} \left(\frac{\hat{v}_r}{b_r(s_r - j\omega)} \boldsymbol{\psi}_0^r \right) \tag{73}$$

and equation (60) yields

$$\underline{\hat{\mathbf{u}}} = \sum_{\underline{r}=1}^{m} \left(\frac{\hat{v}_{\underline{r}}}{b_{\underline{r}}(s_{\underline{r}} - j\omega)} \underline{\boldsymbol{\psi}_0^r} \right). \tag{74}$$

4.4.2. *Case* 2: $\mathscr{R}_1$ *is not negligible*

The modal superposition is

$$\hat{\mathbf{u}}(\omega) = [\boldsymbol{\psi}_0]\hat{\boldsymbol{\zeta}}(\omega) \tag{75}$$

with $\hat{\boldsymbol{\zeta}}(\omega)$ the solution of

$$[\boldsymbol{\Lambda}]^{d-1}[\boldsymbol{\psi}_0]^t\hat{\mathscr{D}}(\omega)[\boldsymbol{\psi}_0]\hat{\mathbf{z}} = [\boldsymbol{\Lambda}]^{d-1}[\boldsymbol{\psi}_0]^t\hat{\mathbf{f}}. \tag{76}$$

Hence, the approximate $\underline{\hat{\mathbf{u}}}$ of $\hat{\mathbf{u}}$ is

$$\underline{\hat{\mathbf{u}}}(\omega) = [\underline{\boldsymbol{\psi}_0}]\underline{\hat{\boldsymbol{\zeta}}}(\omega) \tag{77}$$

with $\underline{\hat{\boldsymbol{\zeta}}}(\omega)$ the solution of

$$[\underline{\boldsymbol{\Lambda}}]^{d-1}[\underline{\boldsymbol{\psi}_0}]^t\hat{\mathscr{D}}(\omega)[\underline{\boldsymbol{\psi}_0}]\underline{\mathbf{z}} = [\boldsymbol{\Lambda}]^{d-1}[\underline{\boldsymbol{\psi}_0}]^t\hat{\mathbf{f}}. \tag{78}$$

The following section is devoted to the application of this technique to the physical problem of poroelastic materials.

5. APPLICATION OF THE GENERALIZED COMPLEX MODES TO THE POROELASTIC PROBLEM

In order to rewrite the poroelastic problem (14) in form (17), a Taylor expansion of $\tilde{\rho}$, $\tilde{\gamma}$, $1/\tilde{\rho}_{22}$ and $1/\tilde{R}$ has to be written. As was said in the introduction, all these coefficients have

the particular property that their dependency is in $j\omega$ and that the low-frequency Taylor expansions have real coefficients. This is very interesting for applying the method of complex modes described in sections 3 and 4.

5.1. ORDER OF TAYLOR EXPANSIONS

In the theoretical part, a construction at order d was presented. For the problem of interest (17), an order must be chosen. Beforehand, a few remarks need to be made. First of all, if one wants to take into account each coefficient, the order of each variable expansion must be greater than 0 or equal to 0. This will lead to a polynomial of degree 4 in ω with valuation equal to 1. This valuation is governed by the coefficient of degree 0 of the expansion of $[\tilde{\mathbf{H}}]$ which is equal to 0. In equation (25), this polynomial is equivalent to a degree 3 polynomial with a valuation equal to 0. This choice is considered. The order of each variable expansion has now to be specified.

Since $[\tilde{\mathbf{M}}]$ is multiplied by $(j\omega)^4$, a zero order Taylor expansion must be performed. $[\tilde{\mathbf{Q}}]$ and $[\tilde{\mathbf{C}}]$ are multiplied by $(j\omega)^2$ and will be expanded at order 2. Finally, for $[\tilde{\mathbf{H}}]$ an order 4 can be chosen. Formally, it can be shown that

$$\tilde{\rho} = ((1-h)\rho_s + h\rho_f) + O(j\omega), \tag{79}$$

$$\frac{1}{\tilde{\rho}_{22}} = \frac{1}{h^2\sigma}(j\omega) - \frac{2\rho_f H + h^2\sigma}{2Hh^4\sigma^2}(j\omega)^2 + \frac{3h^4\sigma^2 + 8\rho_f^2H^2 + 8h^2\sigma\rho_f H}{8H^2h^6\sigma^3}(j\omega)^3$$

$$- \frac{5h^6\sigma^3 + 16h^4\sigma^2\rho_f H + 16\rho_f^3H^3 + 24\rho_f^2H^2h^2\sigma}{16H^3h^8\sigma^4}(j\omega)^4 + O((j\omega)^5), \tag{80}$$

$$\tilde{\gamma} = -1 + \frac{\rho_{12} + \rho_f}{h\sigma}j\omega - \frac{(\rho_f + \rho_{12})(2\rho_f H + h^2\sigma)}{2Hh^3\sigma^2}(j\omega)^2 + O((j\omega)^3), \tag{81}$$

$$\frac{1}{\tilde{R}} = \frac{1}{hP_0} - \frac{2(\gamma-1)}{h\gamma P_0 H'}(j\omega) + 5\frac{\gamma-1}{h\gamma P_0 H'^2}(j\omega)^2 + O((j\omega)^3). \tag{82}$$

Figure 2 presents the relative differences between the value of each parameter and its Taylor expansion versus frequency for the three materials presented in section 5 in the frequency range [0; 1500 Hz]. One can observe that all the relative differences are lower than 10^{-3} which shows the validity of this development and the good approximation of the matrix of operator $\mathscr{D}$ in equation (24) by using a *development at order* 4.

5.2. STUDY OF $\mathscr{R}_d$

Regarding $\mathscr{R}_d$ a few points need to be explained. $\mathscr{R}_d$ is the difference between operator whose modes are calculated and operator $\mathscr{D}$ of equation (49) on which the forcing is applied. In the case of poroelastic materials $\mathscr{R}_d$ is made up of three terms as

$$\mathscr{R}_d = \mathscr{R}_{exp} + \mathscr{R}_{\eta_s} + \mathscr{R}_f. \tag{83}$$

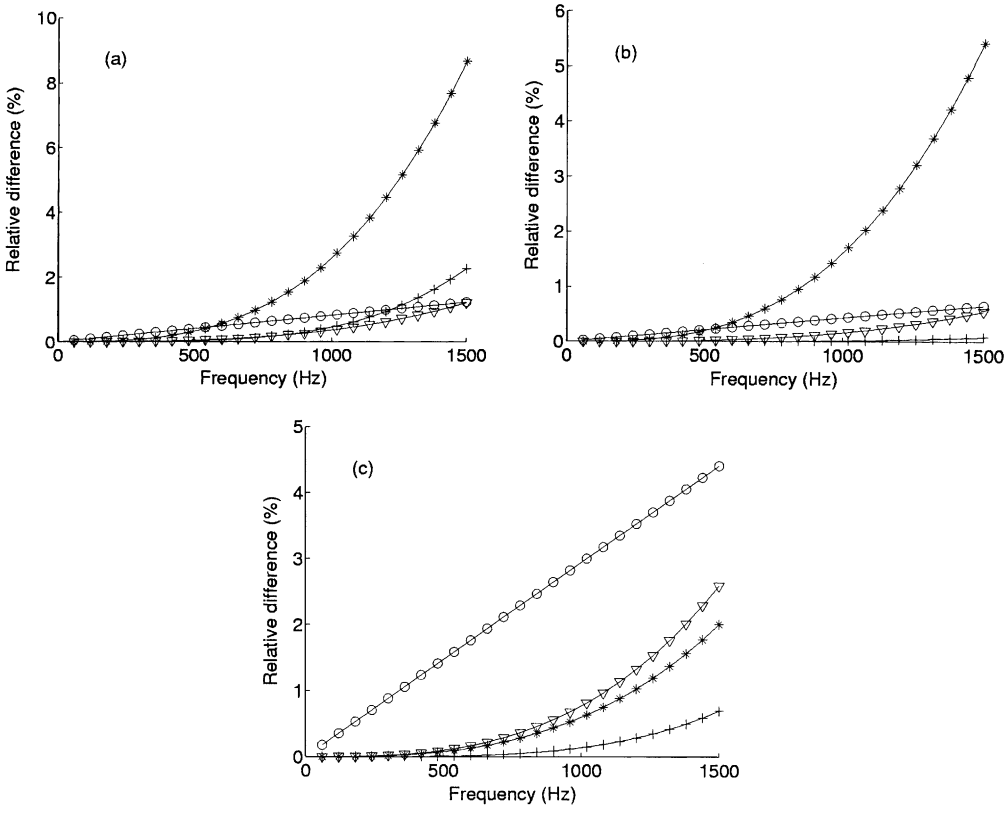

Figure 2. Relative difference between parameter and their Taylor expansion: (a) material A; (b) material B; (c) material C; —○—, $10^4 \Delta_r(\tilde{\rho})$; —+—, $10^5 \Delta_r(1/\tilde{\rho}_{22})$; —▽—, $10^5 \Delta_r(1/\tilde{R})$; —*—, $10^4 \Delta_r(\tilde{\gamma})$.

$\mathscr{R}_{exp}$ is due to the *remainder at order d* in the expansion of operator $\mathscr{D}$ in equation (24). This is supposed to decrease with the order of expansions. Nevertheless, numerical results (detailed in the former section) can let one suppose that its influence on the result can be neglected.

$\mathscr{R}_{\eta_s}$ is due to the approximation made by neglecting the structural damping in the stiffness matrix of the solid phase during the research of the modes.

$\mathscr{R}_f$ is due to the way forcing terms are numerically implemented. In the case of porous materials acoustically or mechanically excited, the forcing is modelled by an imposition of different degree of freedom (for example, a mechanical excitation consists in imposing the displacement of the solid face nodes on the interface where the excitation is applied). Numerically, this imposition can be performed by the following method inspired by reference [32]. Let $[\mathbf{M}(\omega)]$ be the (n, n) matrix of operator D envisaged in equation (49) and $\bar{\mathbf{u}}$ the vector of imposed d.o.f. where the ith coefficient is equal to 0 if no imposition is made on the corresponding d.o.f. and equal to the imposed value in the case of a prescribed d.o.f. The forcing $\mathbf{f}$ is applied so that its ith component is equal to 0 if the corresponding d.o.f. is not imposed. $[\mathbf{M}(\omega)]$ is replaced by $[\overline{\mathbf{M}(\omega)}]$ constructed by putting a 0 on each row and column corresponding to an imposed d.o.f. (e.g., d.o.f. i) except for the coefficient of index (i, i) where the value β_i is put. One gets

$$[\overline{\mathbf{M}(\omega)}] = [\mathbf{M}(\omega)] + \mathscr{R}_f. \tag{84}$$

This can be written explicitly as

$$[\mathbf{M}(\omega)] = \begin{bmatrix} M_{11}(\omega) & & M_{1i}(\omega) & & \\ & \ddots & \vdots & & \\ M_{i1}(\omega) & \cdots & M_{ii}(\omega) & \cdots & M_{in}(\omega) \\ & & \vdots & \ddots & \\ & & M_{ni}(\omega) & & M_{nn}(\omega) \end{bmatrix},$$

$$[\overline{\mathbf{M}(\omega)}] = \begin{bmatrix} M_{11}(\omega) & & 0 & & \\ & \ddots & \vdots & & \\ 0 & \cdots & \beta_i & \cdots & 0 \\ & & \vdots & \ddots & \\ & & 0 & & M_{nn}(\omega) \end{bmatrix}. \tag{85}$$

Hence, the sought solution $\{u\}$ is the one of

$$[\overline{\mathbf{M}(\omega)}] \begin{Bmatrix} u_1 \\ \vdots \\ u_i \\ \vdots \\ u_n \end{Bmatrix} = \begin{Bmatrix} -\sum_i m_{1i}\overline{u_i} \\ \vdots \\ \beta_i \overline{u_i} \\ \vdots \\ -\sum_i m_{ni}\overline{u_i} \end{Bmatrix}. \tag{86}$$

5.3. MODAL REDUCTION

As underlined previously, the *reduction property* is the only one that can be used and a truncation procedure of a modal family must be elaborated now. The method proposed here is based on the analysis of the *nd* eigenvalues of equation (30).

First of all, modes corresponding to $s_r = -\alpha_r + j\omega_r$ with $\alpha_r < 0$ need to be discarded for the physical reason that they do not correspond to damped materials.

Then, by looking at equation (73) it can be noticed that at pulsation ω, the norm of the contribution of mode r is given by

$$|\hat{z}_r| = \frac{|\hat{v}_r|}{b_r\sqrt{\alpha_r^2 + (\omega_r - \omega)^2}}. \tag{87}$$

Regarding modes with $\omega_r \neq 0$, one can define $\xi_r = \alpha_r/\omega_r$ and equation (87) becomes

$$|\hat{z}_r| = \frac{|\hat{v}_r|}{b_r\sqrt{\omega_r^2\,\xi_r^2 + (\omega_r - \omega)^2}}. \tag{88}$$

The principle of the criterion is, over a given spectrum, to give two values ξ_c and ω_c which delimit the set of the selected eigenvalues. Modes with $\omega_r > \omega_c$ or modes with $\xi_r > \xi_c$ are not kept in the expansions.

Regarding the real modes (i.e., with $\omega_r = 0$), it can be suggested to drop modes that satisfy $|\alpha_r| > \alpha_c = \xi_c\omega_c$.

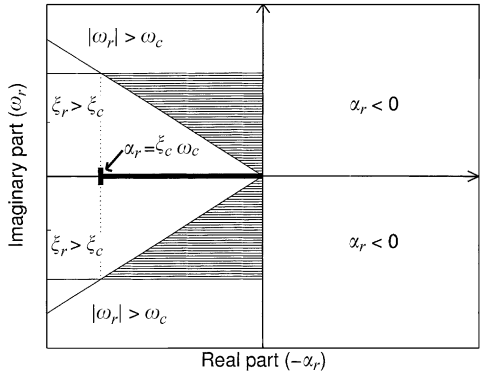

Figure 3. Admissible values of $s_r = -\alpha_r + j\omega_r$; the hachured set corresponds to the complex admissible values and the thick line on the abscissa-axis corresponds to the admissible real modes.

TABLE 1

Samples characteristics

Sample	Material A	Material B	Material C
Flow resistivity, σ (kN/m^4 s)	87	40	25
Porosity, h	0·97	0·94	0·95
Tortuosity, α_∞	2·52	1·06	1·4
Viscous characteristic length, Λ (m)	37×10^{-6}	56×10^{-6}	$93{\cdot}2 \times 10^{-6}$
Thermal characteristic length, Λ' (m)	119×10^{-6}	110×10^{-6}	93.2×10^{-6}
The Poisson's coefficient, v	0·3	0	0
In vacuo shear's modulus, N (kPa)	55	2200	21
Structural damping coefficient, η_s	0·055	0·1	0·05
Solid density, ρ_1 (kg/m^3)	31	130	30

These considerations lead one to discard all modes whose eigenvalue does not pertain to the set X of $\mathbb{C}$, depicted in Figure 3.

The theoretical construction of this set is not so simple to determine in the case of porous materials due to the dependence of the variables of the model on many physical parameters; nevertheless, the following section shows preliminary results regarding the establishment of such limits.

6. NUMERICAL EXAMPLES

6.1. STUDIED CASES

The method presented is tested and compared to the direct solution of the system. Linear shape functions $[\mathbf{N}^u]$ and $[\mathbf{N}^p]$ were used in the finite-element implementation. Three porous material (A, B, C) are considered whose characteristics are given in Table 1. The characteristics of these materials are different enough to show the convergence of the method in very distinct cases.

To test the approach, a mono-dimensional finite-element model has been developed. The thickness of the sample is 0·12 m. The mesh consists of 25 nodes along the thickness which

ensures the convergence of the indicators of interest. It is assumed to be bonded at one end. This leads to a 49 d.o.f.'s problem. The sample is submitted to two different kinds of excitation in the frequency band [0; 1500 Hz]. The first one is called mechanical and consists in imposing a prescribed value on the displacement of the solid-phase node at the surface of excitation. In this case it consists of a harmonic displacement at pulsation ω of amplitude 10^{-8} m. The second one is called acoustical and consists in imposing the pressure in the pores of the fluid phase at the surface of excitation (a harmonic variation of the pressure of pulsation ω and amplitude 1 Pa). These loads are in the domain of application of all the physical models used in the paper.

For these configurations, numerical validations lies in the comparison between the solution given by the generalized complex modes and the solution obtained in terms of physical coordinates. The solutions are compared through two specific vibro-acoustics indicators: the mean square velocity of the solid phase given by equation (89) which is a quadratic average of the velocity in the solid phase of the porous medium and the mean square pressure in the pores of the fluid phase given by equation (90) which is a quadratic average of the pressure in the fluid phase pores of the sample. The expressions for the indicators are, respectively,

$$\langle v^2 \rangle = \frac{\omega^2}{2\Omega_p} \int_{\Omega_p} |u^2(M)| \mathrm{d}\Omega(M) = \frac{\omega^2}{2\Omega_p} \bar{\mathbf{u}}^{\mathrm{t}} [\mathbf{M}_{int}] \mathbf{u} \tag{89}$$

and

$$\langle P^2 \rangle = \frac{1}{2\Omega_p} \int_{\Omega_p} |P^2(M)| \mathrm{d}\Omega(M) = \frac{\rho_0 c_0^2}{2\Omega_p} \bar{\mathbf{P}}^{\mathrm{t}} [\mathbf{Q}_{int}] \mathbf{P}. \tag{90}$$

6.2. GENERALIZED COMPLEX MODES

This section is dedicated to the investigation of the calculated coupled complex modes. This is the first time that poroelastic modes including viscous and thermal damping in both phases and coupling between them have been presented. These modes are calculated without any constraints on the face where the excitation is applied. They can then be called *free modes.*

6.2.1. *Modes with* $\omega_r \neq 0$

Consider the complex modes with complex eigenvalues. Table 2 shows the different eigenfrequencies of the five first coupled complex modes of each sample. The first two

TABLE 2

Calculated eigenfrequencies of the coupled modes (Hz)

Mode	A	B	C
1	291	441	57
2	513	1304	260
3	819	2166	433
4	1091	3034	604
5	1370	3589	774

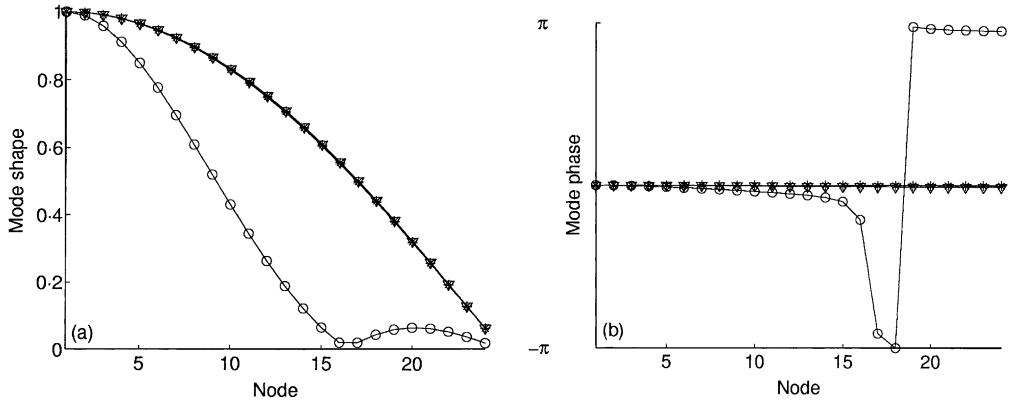

Figure 4. Mode 1, solid phase: (a) mode shape, (b) mode phase. —○—, material A; —+—, material B; —▽—, material C; —∗—, undamped and uncoupled.

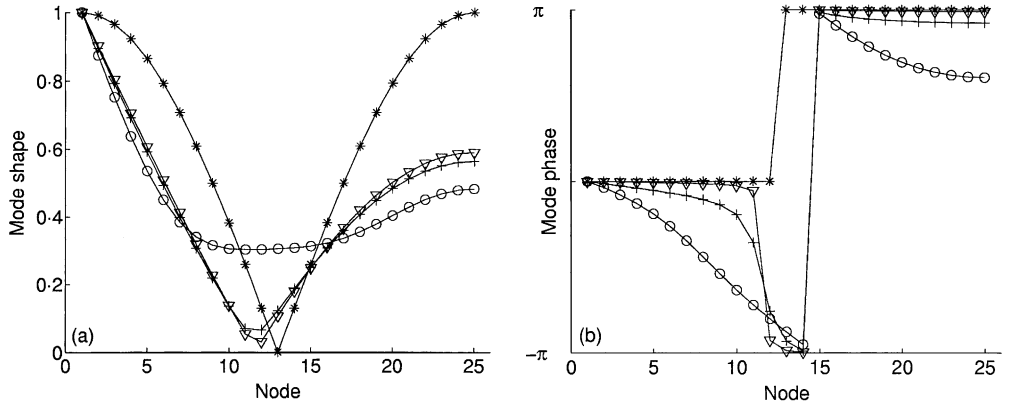

Figure 5. Mode 1, fluid phase: (a) mode shape; (b) mode phase, —○—, material A; —+—, material B; —▽—, material C; —∗—, undamped and uncoupled.

modes for each sample (i.e., the modes with the lowest imaginary part) are considered. Figures 4–7 present the norm and the phase of those modes. To have more readable graphics, modes are shown with a maximum value of the norm equal to 1 and an initial phase equal to 0. The modal shapes and phase for both the solid and fluid phases are shown for the three materials. In addition, the undamped and uncoupled modes calculated by Sgard *et al.* [20] are also plotted.

Figures 4 and 5 present the norm and the phase of the first mode. One can see in Figure 4 that the first modal form (norm and shape) of the solid phase is very similar for B and C and is identical to the first mode calculated when neglecting coupling and damping mechanisms. Material A exhibits notable differences. Regarding the fluid phase one can observe more noticeable discrepancies, especially differences occur for materials B and C.

Figures 6 and 7 show the norm and the phase of the second mode. One can observe that dissimilarities between the different materials are more important compared to the first mode.

These results yield the following observations: the fluid phase seem more dependent on the introduction of damping terms than the solid phase, and these differences have a more noticeable influence on the modal phase than the modal shape. Furthermore, differences increase with the order of the modes. Indeed, since the eigenfrequency increases with the

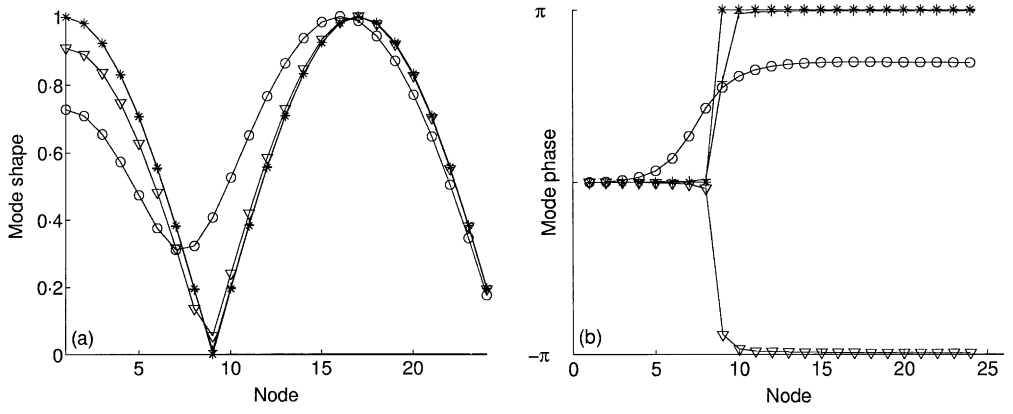

Figure 6. Mode 2, solid phase: (a) mode shape; (b) mode phase, —○—, material A; —+—, material B; —▽—, material C; —*—, undamped and uncoupled.

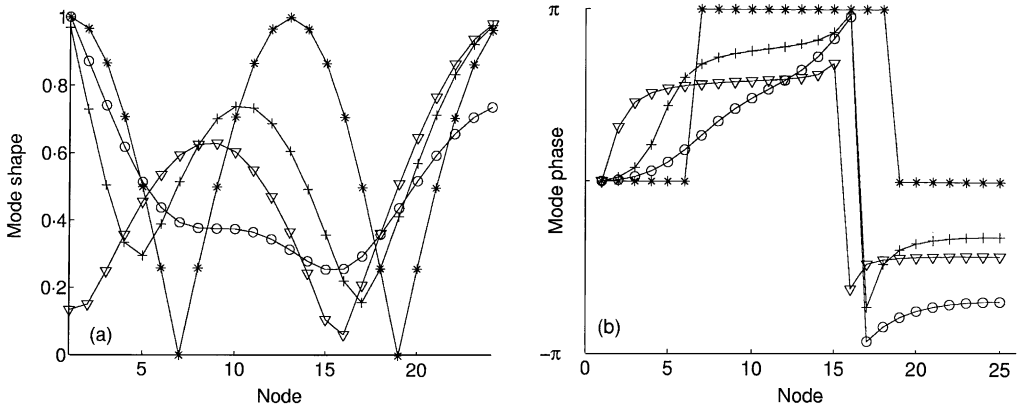

Figure 7. Mode 2, fluid phase: (a) mode shape; (b) mode phase, —○—, material A; —+—, material B; —▽—, material C; —*—, undamped and uncoupled.

order of the modes, the dissipative effects are more and more important and then their influence on modes are more perceptible.

6.2.2. *Modes with* $\omega_r = 0$

This part of the analysis is relative to the purely real modes. Contrary to materials B and C, material A presents the particularity to have a mode with a real negative eigenvalue whose value is of the order of one of the first complex modes. Numerically, it will be shown that this mode has to be taken into account in the modal superposition. This mode is presented in Figure 8.

6.3. MODAL SUPERPOSITION

6.3.1. *Reduction*

The purpose of this part is to validate the approach by showing the convergence of the modal superposition on the [0; 1500 Hz] frequency band for both excitations defined

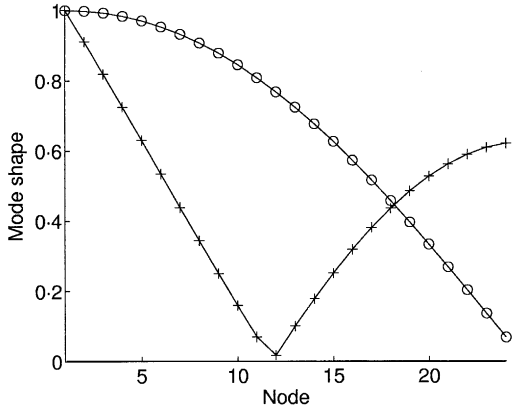

Figure 8. Material A, real mode 1. —○—, solid phase; —+—, fluid phase.

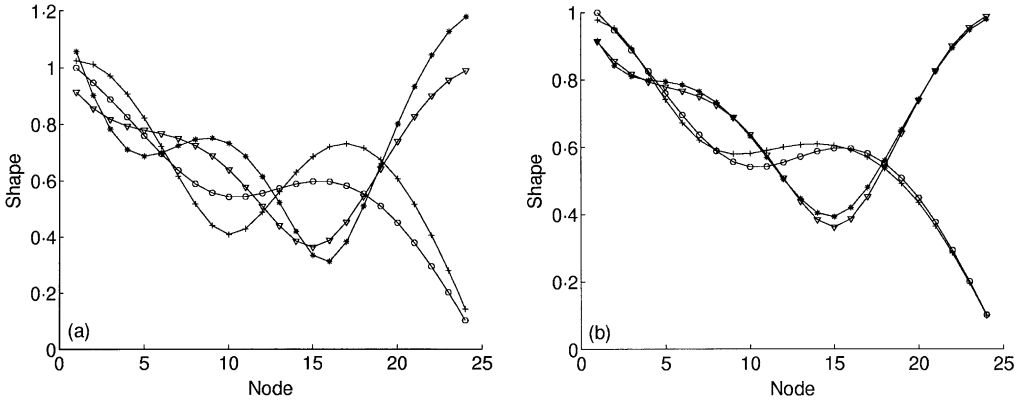

Figure 9. Material C, mechanical excitation, 250 Hz: (a) unsplit modes; (b) split modes, —○—, solid phase, direct; —+—, solid phase, modal; —▽—, fluid phase, direct; —*—, fluid phase, modal.

previously. Figures 10–15 present the comparison between the modal solution and the reference obtained by a direct resolution of the system. These diagrams represent the vibro-acoustic indicators defined previously (in dB) versus frequency.

To discard convergence problems during the projection process, the solid and fluid parts of generalized complex mode are split. Each selected mode generates two vectors. The first one contains only the solid d.o.f.'s and is completed by zeros at the location of fluid d.o.f.'s. The second one is constructed similarly for the fluid phase. To illustrate this fact, the comparison between the proposed approach and the direct one is tested for the solid displacement and the fluid-phase pressure along the thickness at frequency 250 Hz. The material investigated is C, excited by a mechanical piston motion. Figure 9 shows the results obtained with the direct projection of modes and with the numerical splitting trick described previously. One can observe that convergence is improved in the second case. This choice led to a doubling of the dimension of the problem to solve (two vectors for one mode).

The purpose is now to prove the reduction property. The following methodology is considered: for each configuration, several simulations are made by increasing the number

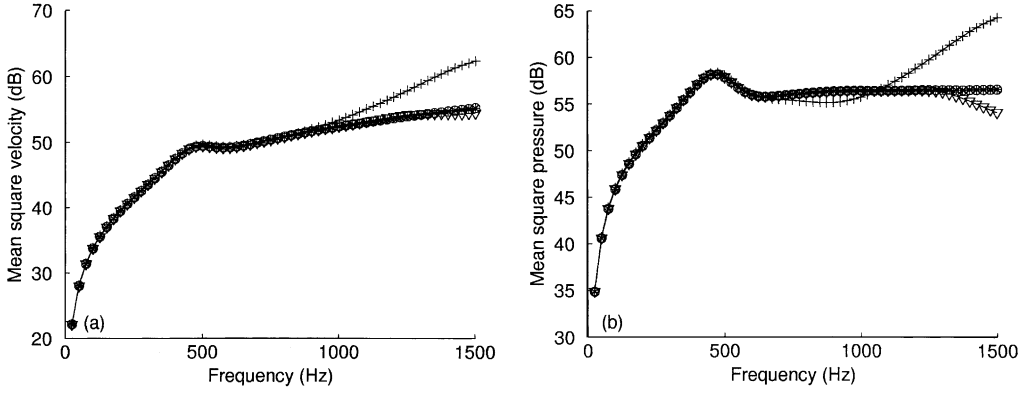

Figure 10. Material A, mechanical excitation amplitude 10^{-8} m: (a) mean square velocity (ref: 5×10^{-8} m/s); (b) mean square pressure (ref: 2×10^{-5} Pa), —○—, direct; —+—, 1 real + 2 complex modes; —▽—, 1 real + 4 complex modes; —∗—, 1 real + 6 complex modes.

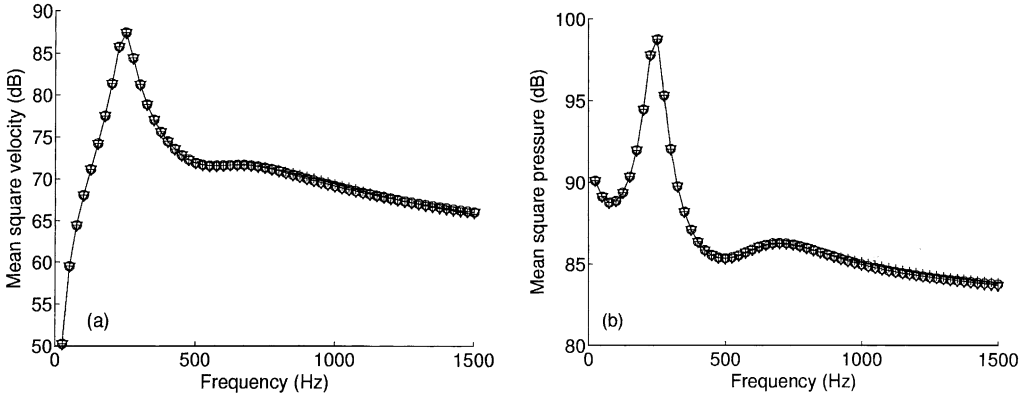

Figure 11. Material A, acoustical excitation amplitude 1 Pa: (a) mean square velocity (ref: 5×10^{-8} m/s); (b) mean square pressure (ref: 2×10^{-5} Pa). —○—, direct; —+—, 2 real + 2 complex modes; —▽—, 2 real + 4 complex modes.

of modes considered in the modal-selected family until obtaining a perfect superposition between the modal and the direct solution. This procedure is incremental and not based on a physical criterion like the one defined in section 5.3. It can be pointed out that, in the modal expansion, an even number of complex modes is needed. Actually, if a given mode is accounted for, its conjugate must also be taken into account, but only one of them needs to be calculated. In addition, with the splitting trick, this number of modes is doubled.

Figure 10 presents the convergence of the mean square velocity and the mean square pressure versus frequency for material A under a mechanical excitation as the number of modes increases. The superposition is made on the modal family constituted by the real mode and the first complex modes. One can see that convergence is good for both indicators up to 1500 Hz with 1 real +6 complex modes and that 1 real +4 complex modes are sufficient to calculate the response up to 900 Hz. Among the six complex modes needed to achieve the convergence up to 1500 Hz, only three have been calculated and the other three are the respective conjugates. Since there is one real and six complex modes, the number of split modes is $2 \times 7 = 14$ which leads to a 14×14 system. This size is to be compared to the otherwise 49×49 problem. Figure 11 presents the convergence of the mean square velocity

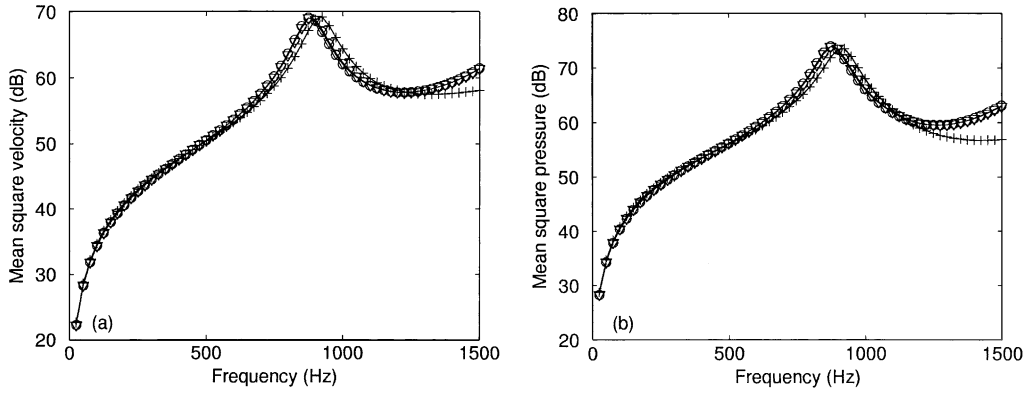

Figure 12. Material B, mechanical excitation amplitude 10^{-8} m: (a) mean square velocity (ref: 5×10^{-8} m/s); (b) mean square pressure (ref: 2×10^{-5} Pa). —○—, direct; —+—, 2 complex modes; —▽—, 4 complex modes.

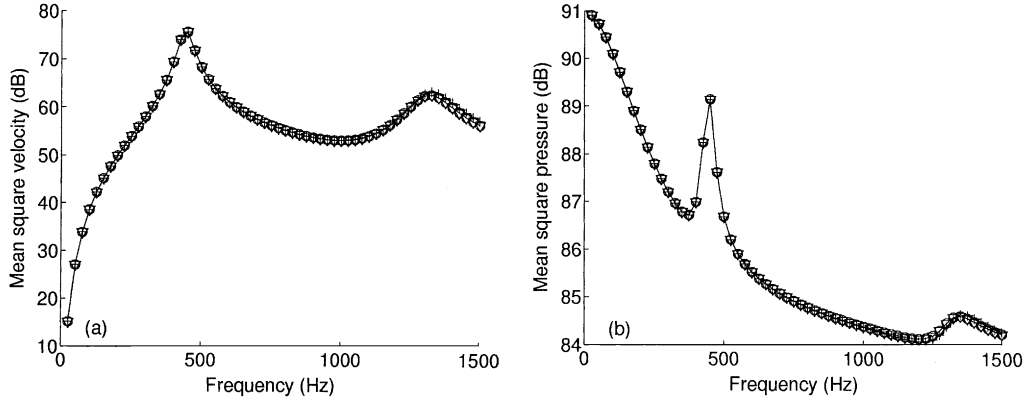

Figure 13. Material B, acoustical excitation amplitude 1 Pa: (a) mean square velocity (ref: 5×10^{-8} m/s); (b) mean square pressure (ref: 2×10^{-5} Pa). —○—, direct; —+—, 1 real + 2 complex modes; —▽—, 1 real + 4 complex modes.

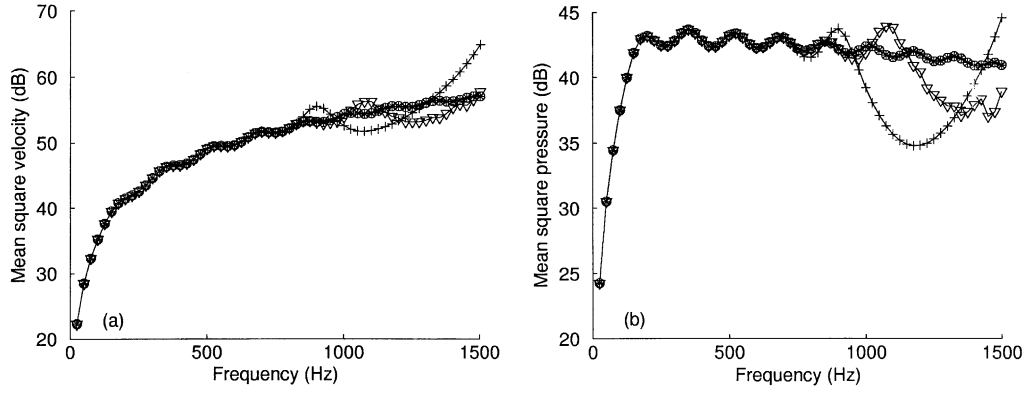

Figure 14. Material C, mechanical excitation amplitude 10^{-8} m: (a) mean square velocity (ref: 5×10^{-8} m/s); (b) mean square pressure (ref: 2×10^{-5} Pa). —○—, direct; —+—, 6 complex modes; —▽—, 8 complex modes; —∗—, 10 complex modes.

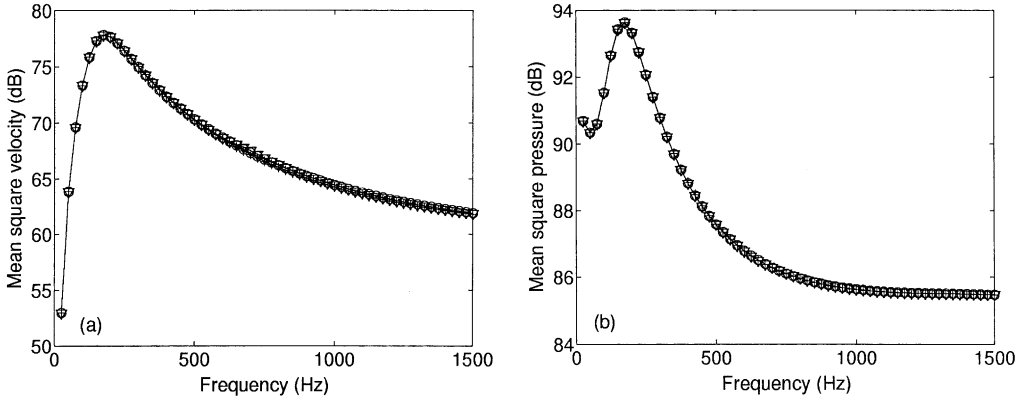

Figure 15. Material C, acoustical excitation amplitude 1 Pa: (a) mean square velocity (ref: 5×10^{-8} m/s); (b) mean square pressure (ref: 2×10^{-5} Pa). —○—, direct; —+—, 1 real + 2 complex modes; —▽—, 1 real + 4 complex modes.

and the mean square pressure versus frequency for material A under an acoustical excitation. For this type of excitation a rigid mode of pressure is added. This one was skipped during the process of mode's calculation because of its null eigenvalue. It is also a real mode so that two real modes need to be accounted for the selected modal family. One can see that convergence is good on all the envisaged spectrum with 2 real +4 complex modes, and the problem to be solved is of size 11×11.

Figures 12–15 present the results obtained for the other configurations. This yields, respectively, to a dimension 8 and 9 problem for material B under a mechanical and acoustical excitation. For material C the sizes are, respectively, 20 (mechanical excitation) and 9 (acoustical excitation).

6.3.2. *Criterion of selections*

One can propose determination of parameters ξ_c and ω_c based on the numerical simulations made for those three materials. This criterion has no general validity and follows from observation.

In order to illustrate the process of selection of the complex modes, consider the following example. For material C under a mechanical excitation, convergence with 6 (resp. 8, 10) modes is good until 700 Hz (resp. 900, 1500 Hz). This amounts to keeping modes whose eigenfrequencies are equal to 604 Hz (resp. 774, 941 Hz). It is unnecessary to mention that if more modes are kept, a better convergence is achieved. Hence, the idea behind the selection process is to keep only all the modes whose imaginary part ω_i is lower than the maximum pulsation ω_{max} of the spectrum so that $\omega_c = \omega_{max}$. This choice has been validated for the other configurations. A proposed value for ξ_c is 0·5. These following choices induce a limit $\alpha_c = \omega_{max}/2$ for real modes.

By looking at the eigenfrequencies and at the numerical simulation of the previous section, this choice can appear over-sized, as shown by the numerical examples; nevertheless, this method and these first investigations can help one to delimit the set of the essential eigenvalues and then the modes to take into account in the modal superposition.

This section was devoted to show the reduction obtained by using the generalized complex modes. The approach has been tested and validated on three different materials

under two types of excitation. A selection procedure has been initiated by looking at the six numerical examples.

7. CONCLUSION

This paper has presented a new modal technique based on complex modes to calculate the vibro-acoustic response of porous materials. This method has the originality to be the first study where frequency non-linearities are introduced in the calculation of poroelastic modes. This non-linearities are induced by various effects in the porous medium which were never introduced before in the calculation of modes to the authors' knowledge (viscous and thermal effects, coupling between solid and fluid phases). Then, it was proved that the calculation of the projection on the generalized complex modes does not depend on the order of the expansions and is equivalent in terms of number of operations to the projection of classical modes. This technique for the first time exhibits coupled and damped modes. This is a preliminary step toward a physical interpretation of those *media behaviors* and opens a door to a better understanding of porous materials. This is a true perspective of this work. Finally, it was shown that using this technique leads to a reduction of the problem.

The main difficulty of this technique lies in the numerical calculation of modes because of the ill-conditioning of matrices and could be the major difficulty in applying this method to a three-dimensional case. The rigorous determination of a selection criterion for modes is also a perspective of this study. Further work involves applying this approach to three-dimensional cases.

REFERENCES

1. R. PANNETON and N. ATALLA 1996 *Journal of Acoustical Society of America* **100**, 346–354. Numerical prediction of sound transmission through multilayer systems with isotropic poroelastic materials.
2. Y. J. KANG and J. S. BOLTON 1995 *Journal of Acoustical Society of America* **98**, 635–643. Finite element modeling of isotropic elastic porous materials coupled with acoustical finite elements.
3. J. P. COYETTE and H. WYNENDAELE 1995 *Proceedings of INTER-NOISE*, Vol. 95, 1279–1282. A finite element model for predicting the acoustic transmission characteristics of layered structures.
4. R. PANNETON and N. ATALLA 1997 *Journal of Acoustical Society of America* **101**, 3287–3298. An efficient finite element scheme for solving the three-dimensional poroelasticity problem in acoustics.
5. R. PANNETON 1996 *Ph.D. Thesis*, *Université de Sherbrooke*. Modélisation Numérique tridimensionelle par éléments finis des milieux poroélastiques.
6. M. A. BIOT 1956 *Journal of Acoustical Society of America* **28**, 168–178. Theory of propagation of elastic waves in a fluid-saturated porous solid. I. Low frequency range.
7. J. F. ALLARD 1993 *Propagation of Sound in Porous Media*, *Modelling Sound Absorbing Materials*. New York: Elsevier Application Science.
8. N. ATALLA, R. PANNETON and P. DEBERGUE 1998 *Journal of Acoustical Society of America* **104**, 1444–1452. A mixed displacement–pressure formulation for poroelastic materials.
9. P. GORANSSON 1995 *Journal of Sound and Vibration* **182**, 479–494. A weighted residual formulation of the acoustic wave propagation through a flexible porous material and a comparison with a limp material model.
10. L. MEIROVITCH 1967 *Analytical Methods in Vibrations*. London: Macmillan Company.
11. H. J.-P. MORAND and R. OHAYON 1995 *Fluid Structure Interaction*. Toronto: John Wiley and Sons.
12. M. C. JUNGER and D. FEIT 1993 *Sound*, *Structures and their Interaction*. Acoustical Society of America through American Institute of Physics.

13. A. KANARACHOS and I. ANTONIADIS 1998 *Journal of Sound and Vibration* **121**, 77–104. Symmetric variational principles and modal methods in fluid-structure interaction problems.
14. M. GERADIN, G. ROBERTS and J. HUCK 1984 *Engineering Computations Journal* **1**, 152–160. Eigenvalue analysis and transient response of fluid-structure problems.
15. H. J.-P. MORAND and R. OHAYON 1979 *International Journal for Numerical Methods in Engineering* **14**, 741–755. Substructure variational analysis of the vibration of coupled fluid-structure systems. Finite element results.
16. F. FAHY 1985 *Sound and Structural Vibration*. London: Academic Press.
17. F. SGARD 1995 *Ph.D. Thesis, Université de Sherbrooke, Insa de Lyon*. Etude numérique du comportement vibroacoustique d'un systeme plaque-cavité dans un écoulement uniforme, pour différents types d'excitation.
18. H. BOUHIOUI 1993 *Ph.D. Thesis, Université Technologique de Compiegne*. Etude vibroacoustique d'un montage en double paroi de verre.
19. H. BOUHIOUI and M. HODGSON 1998 135*th Meeting of the Acoustical Society of America, Seattle, U.S.A*. Finite-element modelling of the vibro-acoustical behaviour of poro-elastic materials.
20. F. SGARD, N. ATALLA and R. PANNETON 1997 134*th Meeting of the Acoustical Society of America, San Diego, U.S.A*. A modal reduction technique for the finite element formulation of biot's poroelasticity equations in acoustics.
21. F. SGARD, N. ATALLA and R. PANNETON 1998 135*th Meeting of the Acoustical Society of America, Seattle, U.S.A*. A modal reduction technique for the finite element formulation of biot's poroelasticity equations in acoustics applied to multilayered structures.
22. C. ZWIKKER and C. W. KOSTEN 1949 *Sound-absorbing Materials*. New York: Elsevier Application Science.
23. D. L. JOHNSON, J. KOPLIK and R. DASHEN 1987 *Journal of Fluid Mechanics* **176**, 379–402. Theory of dynamic permeability and tortuosity in fluid-saturated porous media.
24. Y. CHAMPOUX 1991 *Ph.D. Thesis, Carleton University*. Etude expérimentale du comportement acoustique des matériaux poreux à structure rigide.
25. W. J. DUNCAN, R. A. FRASER and A. R. COLLAR 1938 *Elementary Matrices and some Applications to Dynamics and Differential Equations*, 289. Cambridge: Cambridge University Press.
26. M. GERADIN and D. RIXEN 1996 *Théorie des Vibrations—Application à la Dynamique des Structures*. Paris: Masson; section 2.3.2.
27. F. CHATELIN 1988 *Valeurs propres de matrices*. Paris: Masson.
28. K.-Y. FUNG, B. HONGBIN JU and B. TALLAPRAGADA 2000 *American Institute of Aeronautics and Astronautics Journal* **38**, 30–38. Impedance and its time-domain extensions.
29. C. K. W. TAM and L. AURIAULT 1996 *American Institute of Aeronautics and Astronautics Journal* **34**, 917–923. Time-domain impedance boundary conditions for computational acoustics.
30. L. MEIROVITCH 1967 *Analytical Methods in Vibrations*. London: Macmillan Company; section 9.7.
31. L. MEIROVITCH 1967 *Analytical Methods in Vibrations*. London: Macmillan Company; section 9.11.
32. O. C. ZIENKIEWICZ 1989 *The Finite Element Method*. London: McGraw-Hill; fourth edition.

APPENDIX A: NOMENCLATURE

vector	$\mathbf{u}$
matrix	$[\mathbf{M}]$
square root of -1	j
degree of freedom	d.o.f.
displacement of solid phase	u
displacement of fluid phase	U
pressure in pores of fluid phase	P
complex conjugate of x	$\bar{x}$
transpose of matrix $[\mathbf{A}]$	$[\mathbf{A}]^{\mathrm{t}}$
set of functions from $\mathbb{R}$ in $\mathbb{C}^n$	$\mathscr{F}(\mathbb{R}, \mathbb{C}^n)$
set of functions from $\mathbb{R}$ in $\mathbb{C}^n$ whose dth derivative is continuous	$\mathscr{C}^d(\mathbb{R}, \mathbb{C}^n)$
selected set of u	$\underline{u}$
relative difference	Δ_r
nabla operator	∇